J|A|C|S
ARTICLES
Published on Web 06/10/2006

Structural Chemistry and Metamagnetism of an Homologous Series of Layered Manganese Oxysulfides

Zoltán A. Gál,[†] Oliver J. Rutt,[†] Catherine F. Smura,[†] Timothy P. Overton,[†] Nicolas Barrier,[†] Simon J. Clarke,*[,†] and Joke Hadermann[‡]

Contribution from the Department of Chemistry, University of Oxford, Inorganic Chemistry Laboratory, South Parks Road, Oxford, OX1 3QR, U.K., and Electron Microscopy for Materials Science (EMAT), University of Antwerp, Groenenborgerlaan 171, B-2020 Antwerp, Belgium

Received February 7, 2006; E-mail: simon.clarke@chem.ox.ac.uk

Abstract: An homologous series of layered oxysulfides $Sr_2MnO_2Cu_{2m-\delta}S_{m+1}$ with metamagnetic properties is described. $Sr_2MnO_2Cu_{2-\delta}S_2$ ($m = 1$), $Sr_2MnO_2Cu_{4-\delta}S_3$ ($m = 2$) and $Sr_2MnO_2Cu_{6-\delta}S_4$ ($m = 3$), consist of MnO_2 sheets separated from antifluorite-type copper sulfide layers of variable thickness by Sr^{2+} ions. All three compounds show substantial and similar copper deficiencies ($\delta \approx 0.5$) in the copper sulfide layers, and single-crystal X-ray and powder neutron diffraction measurements show that the copper ions in the $m = 2$ and $m = 3$ compounds are crystallographically disordered, consistent with the possibility of high two-dimensional copper ion mobility. Magnetic susceptibility measurements show high-temperature Curie−Weiss behavior with magnetic moments consistent with high spin manganese ions which have been oxidized to the $(2+\delta)^+$ state in order to maintain a full Cu-3*d*/S-3*p* valence band, and the compounds are correspondingly *p*-type semiconductors with resistivities around 25 Ω cm at 295 K. Positive Weiss temperatures indicate net ferromagnetic interactions between moments. Accordingly, magnetic susceptibility measurements and low-temperature powder neutron diffraction measurements show that the moments within a MnO_2 sheet couple ferromagnetically and that weaker antiferromagnetic coupling between sheets leads to *A*-type antiferromagnets in zero applied magnetic field. $Sr_2MnO_2Cu_{5.5}S_4$ and $Sr_2MnO_2Cu_{3.5}S_3$ are metamagnets which may be driven into the fully ordered ferromagnetic state below 25 K by the application of fields of 0.06 and 1.3 T respectively. The relationships between the compositions, structures, and physical properties of these compounds, and the prospects for chemical control of the properties, are discussed.

Introduction

The chemistry and physics of solid-state compounds with layered structures is often quite different from that of compounds with isotropic structures.[1−3] Low-dimensional structures are often favored when the anions are polarizable,[4] and there are more examples of layered sulfides than there are of layered oxides. The layered nature of sulfides can be reinforced if two different metal cations are incorporated which have different chemical requirements.[5] A more extreme way of enforcing a layered crystal structure is to choose compounds in which the chemical preferences and/or coordination requirements of *both* the cation- and anion-forming elements are different. While this approach is not guaranteed to lead to a single-phase compound, there are many examples of, for example, oxychalcogenides and oxypnictides where it is successful. The results are compounds with complex crystal structures composed of distinct oxide and chalcogenide or pnictide layers which may form an homologous series.[6]

Layered oxychalcogenides of current interest include the *Ln*OCuS[7,8] series (*Ln* = lanthanide) composed of alternating Ln_2O_2 fluorite layers and Cu_2S_2 antifluorite layers: $La_{1-x}Sr_xOCuS$ is a rare example of a transparent *p*-type semiconductor[9] in which the Cu-3*d*/S-3*p* valence band is doped with holes. Related copper sulfide antifluorite layers are found in the more complex homologous series of compounds described in this paper which also contain strontium manganese oxide layers. Figure 1 shows the idealized crystal structures of a series of such compounds.[10−13] To emphasize the layered nature of these compounds we will write the formulas so as to reflect the compositions of the distinct oxide and sulfide layers.

[†] University of Oxford.
[‡] University of Antwerp.

(1) Canadell, E.; Whangbo, M. H. *Chem. Rev.* **1991**, *91*, 965.
(2) Rouxel, J.; Brec, R. *Annu. Rev. Mater. Sci.* **1986**, *16*, 137.
(3) deJongh, L. J. *Magnetic Properties of Layered Transition Metal Compounds*; Kluwer Academic Publishers: Dordrecht, 1990.
(4) Madden, P. A.; Wilson, M. *Chem. Soc. Rev.* **1996**, 339.
(5) Meerschaut, A. *Curr. Opin. Solid State Mater. Sci.* **1996**, *1*, 250.
(6) Cava, R. J.; Zandbergen, H. W.; Krajewski, J. J.; Siegrist, T.; Hwang, H. Y.; Batlogg, B. *J. Solid State Chem.* **1997**, *129*, 250.
(7) Ueda, K.; Inoue, S.; Hirose, S.; Kawazoe, H.; Hosono, H. *Appl. Phys. Lett.* **2000**, *77*, 2701.
(8) Hiramatsu, H.; Kamioka, H.; Ueda, K.; Hirano, M.; Hosono, H. *J. Ceram. Soc. Jpn.* **2005**, *113*, 10.
(9) Takano, Y.; Yahagi, K.; Sekizawa, K. *Physica B* **1995**, *206−207*, 764.
(10) Barrier, N.; Clarke, S. J. *Chem. Commun.* **2003**, 164.
(11) Zhu, W. J.; Hor, P. H. *J. Solid State Chem.* **1997**, *130*, 319.
(12) Zhu, W. J.; Hor, P. H. *J. Solid State Chem.* **2000**, *153*, 26.
(13) Zhu, W. J.; Hor, P. H. *J. Solid State Chem.* **1997**, *134*, 128.

10.1021/ja060892o CCC: $33.50

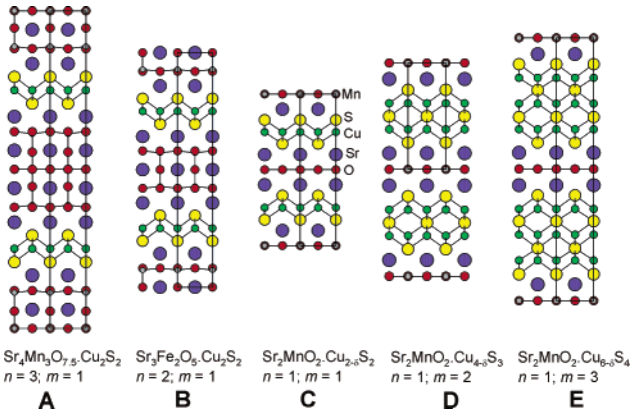

Figure 1. Idealized structures of the homologous series of compounds $Sr_{n+1}M_nO_{3n-1}Cu_{2m}S_{m+1}$, mostly represented by compounds in which M = Mn. Compounds **D** and **E** are described here for the first time together with new measurements on compound **C**.[11] (Color key: Sr: blue; Mn/Fe: gray; O: red; Cu: green; S: yellow).

The homologous series $Sr_{n+1}M_nO_{3n-1}Cu_{2m}S_{m+1}$ (where M is a transition metal) is represented by the n = 1, 2, 3; m = 1 members in which Cu_2S_2 antifluorite layers (which we refer to as "single" copper sulfide layers) are separated either by Sr_2MO_2 layers containing MO_2 sheets (n = 1), as in numerous examples of compounds $Sr_2MO_2Cu_2S_2$ (M = Mn,[11] Co,[14−16] Ni,[17] Cu,[17] Zn[11,18,19]) (**C** in Figure 1), or by thicker oxide layers which resemble fragments of the perovskite structure: $Sr_3M_2O_5Cu_2S_2$ (**B**) (n = 2; M = Fe,[13] Sc[17]) and $Sr_4Mn_3O_{7.5}Cu_2S_2$ (**A**) (n = 3).[12] Here we introduce the new n = 1; m = 2, 3 manganese-containing members of the series (**D** and **E**) containing "double"- and "triple"-thickness copper sulfide layers respectively, and provide further analysis of the n = 1, m = 1 member $Sr_2MnO_2Cu_{2-\delta}S_2$ (**C**).[11] These n = 1 members of the homologous series $Sr_{n+1}M_nO_{3n-1}Cu_{2m}S_{m+1}$ will be referred to by their m indices. $Sr_4Mn_2O_4Cu_5S_5$,[10] a 1:1 intergrowth of the m = 1 and m = 2 members, hints that a more complex series of intergrowth phases of this type may be attainable.

Property measurements on $Sr_2MnO_2Cu_2S_2$[11] (n = 1; m = 1) and isostructural relatives reveal complex chemistry and physics. The reported susceptibility measurements of $Sr_2MnO_2Cu_2S_2$[11] suggest three-dimensional antiferromagnetic ordering of manganese moments. The semiconducting cobalt-containing analogue $Sr_2CoO_2Cu_2S_2$[14−16] also shows long-range antiferromagnetic ordering, but also more complex electronic behavior indicating a strong correlation between charge transport and the magnetic state[20] which has yet to be fully resolved. In contrast, the n = 1; m = 1 oxypnictides $A_2MnO_2Zn_2As_2$[21−24] are spin glasses with no long-range magnetic order. Investigations of the n = 2; m = 1 and n = 3; m = 1 representatives of the $Sr_{n+1}M_nO_{3n-1}Cu_{2m}S_{m+1}$ homologous series, $Sr_3Fe_2O_5Cu_2S_2$,[13] and $Sr_4Mn_3O_{7.5}Cu_2Ch_2$ (Ch = S, Se)[12] reveal that these Mott−Hubbard insulators show low dimensional antiferromagnetic ordering. The properties of the analogous band gap insulators such as $Sr_2ZnO_2Cu_2S_2$[11] are, like those of LaOCuS, dominated by the ease of depletion of the antibonding states at the top of the Cu-3*d*/S-3*p* valence band. Hole doping, achieved by substituting 5% Na^+ for Sr^{2+} in $Sr_2ZnO_2Cu_2S_2$, has been shown to enhance the conductivity by 7 orders of magnitude.[19] The layered oxychalcogenides and oxypnictides of the 1st row transition metals exhibit a range of properties and present numerous, as yet largely unexploited, opportunities for control of the magnetic and electronic transport properties via ionic substitutions on many of the crystallographic sites.

Although $Sr_4Mn_2O_4Cu_5S_5$,[10] is the first of these oxysulfide intergrowths to be reported containing $[Cu_{2m}Ch_{m+1}]^{2-}$ layers with m > 1, several ternary chalcogenides contain these structural fragments, notably $TlCu_{2m}S_{m+1}$ (m = 1,[25] 2,[26] 3[27]), $TlCu_{2m}Se_{m+1}$ (m = 1,[28] 2[26]), ACu_4S_3 (A = K,[29] Rb,[30] Cs[31]) and ACu_4Se_3 (A = K, Rb, Cs[26,32]). These all formally contain $[Cu_{2m}S_{m+1}]^-$ monoanionic layers, and this implies the existence of one hole per formula unit in the Cu-3*d*/S-3*p* valence band. Conductivity measurements show these compounds to be metallic[29] and calculations on these layers[33] suggest that such holes should be mobile in the $[Cu_{2m}S_{m+1}]^-$ layers due to large Cu-3*d*/S-3*p* overlap. In the oxysulfide intergrowth compounds reported here, the structural, magnetic and electronic properties will be determined by the geometry of the transition metal cation in the oxide layer, the structural demands of both the oxide and sulfide layers, and the electronic communication between the oxide and sulfide layers. Here we discuss the correlation between the compositions, crystal structures and properties of the m = 1, m = 2, and m = 3 members of the homologous series $Sr_2MnO_2Cu_{2m-\delta}S_{m+1}$.

Experimental Section

Synthesis of $Sr_2MnO_2Cu_{2m-\delta}S_{m+1}$ (m = 1, 2, 3). The products of these reactions are air stable, however moisture-sensitive reactants required a drybox (combined O_2 and H_2O content < 1 ppm) for manipulations of solids. Starting materials were: MnO_2 powder (ALFA 99.999%), Cu powder (ALFA 99.9995%), Mn flake (Aldrich 99.99%) ground into powder, CuO powder (ALFA 99.99%). SrS was synthesized by the reaction at 800 °C for 8 h between $SrCO_3$ powder (ALFA 99.994%) and CS_2 (Aldrich 99.5%) vapor (details and safety precautions are detailed elsewhere[34]). Cu_2S was prepared by reacting copper powder with sulfur (ALFA 99.9995%) in a dried evacuated sealed silica tube

(14) Zhu, W. J.; Hor, P. H.; Jacobson, A. J.; Crisci, G.; Albright, T. A.; Wang, S.-H.; Vogt, T. *J. Am. Chem. Soc.* **1997**, *119*, 12398.
(15) Matoba, M.; Takeuchi, T.; Okada, S.; Kamihara, Y.; Itoh, M.; Ohoyama, K.; Yamaguchi, Y. *Physica B* **2002**, *312−313*, 630.
(16) Okada, S.; Matoba, M.; Fukumoto, S.; Soyano, S.; Kamihara, Y.; Takeuchi, T.; Yoshida, H.; Ohoyama, K.; Yamaguchi, Y. *J. Appl. Phys.* **2002**, *91*, 8861.
(17) Otzschi, K.; Ogino, H.; Shimoyama, J.; Kishio, K. *J. Low Temp. Phys.* **1999**, *117*, 729.
(18) Hirose, H.; Ueda, K.; Kawazoe, H.; Hosono, H. *Chem. Mater.* **2002**, *14*, 1037.
(19) Ueda, K.; Hirose, S.; Kawazoe, H.; Hosono, H. *Chem. Mater.* **2001**, *13*, 1880.
(20) Okada, S.; Terasaki, I.; Ooyama, H.; Matoba, M. *J. Appl. Phys.* **2004**, *95*, **6816.**
(21) Brock, S. L.; Raju, N. P.; Greedan, J. E.; Kauzlarich, S. M. *J. Alloys Compd.* **1996**, *237*, 9; Brock, S. L.; Kauzlarich, S. M. *J. Alloys Compd.* **1996**, *241*, 82.
(22) Ozawa, T. C.; Olmstead, M. M.; Brock, S. L.; Kauzlarich, S. M.; Young, D. M. *Chem. Mater.* **1998**, *10*, 392.
(23) Matsushita, A.; Ozawa, T. C.; Tang, J,; Kauzlarich, S. M. *Physica B* **2000**, *284−288*, 1424.
(24) Ozawa, T. C.; Kauzlarich, S. M.; Bieringer, M.; Wiebe, C. R.; Greedan, J. E.; Gardner, J. S. *Chem. Mater.* **2001**, *13*, 973.
(25) Berger, R. *J. Less Common Met.* **1989**, *147*, 141.
(26) Klepp, K. O.; Boller, H.; Voellenkle, H. *Monatsh. Chem.* **1980**, *111*, 727.
(27) Berger, R.; Eriksson, L. *J. Less Common Met.* **1990**, *161*, 165.
(28) Berger, R.; van Bruggen, C. F. *J. Less Common Metals* **1984**, *99*, 113.
(29) Brown, D. R.; Zubieta, J. A.; Vella, P. A.; Wrobleski, J. T.; Watt, T.; Hatfield. W. E.; Day, P. *Inorg. Chem.* **1980**, *19*, 1945.
(30) Ruedorff, W.; Schwarz, H. G.; Walter, M. *Z. Anorg. Allg. Chem.* **1952**, *269*, 141.
(31) Burschka, C. *Z. Anorg. Allg. Chem.* **1980**, *463*, 65.
(32) Hartig, N. S.; Dorhout, P. K.; Miller, S. M. *J. Solid State Chem.* **1994**, *113*, 88.
(33) Vajenine, G. V.; Hoffmann, R. *Inorg. Chem.* **1996**, *35*, 451.
(34) Broadley, S.; Gál, Z. A.; Corà, F.; Smura, C. F.; Clarke, S. J. *Inorg. Chem.* **2005**, *44*, 9092.

for 12 h at 400 °C, followed by a further 4 days at 700 °C. SrO was prepared by decomposing $SrCO_3$ under dynamic vacuum at 900 °C for 24 h with a final firing of 3 h at 1100 °C. The quinary products were obtained as bulk powders on the 1−10 g scale by grinding stoichiometric quantities of the reactants thoroughly in an agate pestle and mortar in the drybox, pressing the mixtures into pellets at 150 MPa and placing the pellets in dry alumina crucibles inside silica tubes that had been baked dry under vacuum for 2−3 h at 1000 °C prior to loading in the drybox. The tubes were sealed under vacuum (10^{-2} mbar) and heated in an electrical resistance chamber furnace at temperatures of 850−1000 °C for 15−20 h followed by cooling at the natural rate of the furnace. Single crystal growth in the pellets was often observed with copper sulfide likely acting as a flux. Single-crystal X-ray analysis was carried out on crystals of $Sr_2MnO_2Cu_{1.5}S_2$ and $Sr_2MnO_2Cu_{3.5}S_3$ made in this way. The highest quality (smallest mosaicity) crystals of $Sr_2MnO_2Cu_{5.5}S_4$ and $Sr_4Mn_2O_4Cu_5S_5$ [10] were obtained when dry KI (ALFA 99.99%) was ground with 0.25 g of the reactant mixture in a 3:1 molar ratio, placed in an alumina crucible inside a baked sealed silica tube and heated at 900 °C for 24 h followed by cooling at 0.1 °Cmin^{-1} to 400 °C prior to removal from the furnace.

Chemical Analysis. Energy dispersive analysis of X-rays (EDX) was carried out on single crystals using a JEOL JSM-840A scanning electron microscope equipped with an Oxford Instruments ISIS300 energy-dispersive X-ray analysis system. It was not possible to obtain quantitative analysis for oxygen using this instrument.

Powder X-ray Diffraction. Measurements were made using a Phillips PW 1729/10 diffractometer operating in Bragg−Brentano geometry with Cu$K\alpha_1/\alpha_2$ radiation and equipped with a diffracted beam monochromator.

Single-crystal X-ray Diffraction. Crystals were mounted in a nylon loop using paratone oil. $Sr_2MnO_2Cu_{3.5}S_3$, $Sr_2MnO_2Cu_{5.5}S_4$, and $Sr_4Mn_2O_4Cu_5S_5$ were measured at 293 K, $Sr_2MnO_2Cu_{1.5}S_2$ was measured at 240 K. Crystals of $Sr_2MnO_2Cu_{3.5}S_3$ and $Sr_2MnO_2Cu_{5.5}S_4$ were also measured between 150 and 200 K either after being cooled rapidly in a few seconds, or more slowly, over a period of about 1 h, using an Oxford Instruments nitrogen gas cooling system. High redundancy data sets were collected on a Nonius Kappa CCD diffractometer using Mo-$K\alpha$ ($\lambda = 0.71073$ Å) radiation. Data reduction[35] was followed by Direct Methods structure solution and full-matrix least-squares refinement with SHELXS97 and SHELXL97 respectively[36] via the WinGX[37] interface. Refinement on F^2 was performed[38] using anisotropic displacement parameters for all atoms. Neutral atom scattering factors and values used to calculate the linear absorption coefficients were taken from the International Tables for X-ray Crystallography.[39] The diffraction data were corrected for Lorentz-polarization and a face indexed numerical[40] absorption correction was applied through the PLATON[41] interface. The absence of additional/missed symmetry was checked by ADDSYM.[42]

Powder Neutron Diffraction. Powder neutron diffraction (PND) data were collected at room temperature using the diffractometer POLARIS at the ISIS Facility, Rutherford Appleton Laboratory, UK. Diffraction patterns were measured by the time-of-flight method in the d-spacing range $0.5 < d < 8$ Å using detector banks at scattering angles 2θ of 35°, 90°, and 145° for a total integrated proton current at the production target of 175 μA·h for 8 g of $Sr_2MnO_2Cu_{1.5}S_2$, 175 μA·h for 8 g of $Sr_2MnO_2Cu_{3.5}S_3$, and 550 μA·h for 2 g of $Sr_2MnO_2Cu_{5.5}S_4$. Data on $Sr_2MnO_2Cu_{3.5}S_3$ and $Sr_2MnO_2Cu_{5.5}S_4$ were also collected at between 5 K and room temperature and in applied magnetic fields on the diffractometer D2B at the Institut Laue-Langevin, Grenoble. Inside either a closed-cycle helium refrigerator or in an Oxford Instruments 5 T vertical field cryomagnet were placed 4−8 g samples. Measurements were made using neutrons of wavelength 1.59 or 2.40 Å in the angular range $5° < 2\theta < 150°$ with a step size of 0.05°. Samples were pressed firmly into the cylindrical vanadium sample can to minimize field-induced preferred orientation. PND data were analyzed using the Rietveld profile refinement suite GSAS.[43] Form factors for magnetic scattering were taken from the International Tables for Crystallography.[39]

Electron Diffraction Measurements. Measurements were carried out on a Phillips CM20 transmission electron microscope with LaB_6 filament. Cooling was performed in situ using a cooling stage with liquid nitrogen, allowing a base temperature of 110 K to be reached.

Magnetic Susceptibility Measurements. Measurements were carried out using Quantum Design MPMS-5 or MPMS-XL SQUID magnetometers in the temperature range 5−300 K and at magnetic fields of up to 7 T. Approximately 20−70 mg of material was weighed accurately into a gelatin capsule. Measurements of the susceptibility were made on warming in measuring fields of between 2.5 mT and 5000 mT after cooling in zero field (zero-field-cooled: ZFC) and then again on warming after cooling in the measuring field (field-cooled: FC). Magnetization isotherms at room temperature were usually slightly nonlinear in the low-field region due to the presence of minuscule amounts of ferromagnetic impurity; the measurement of the true bulk susceptibility of the sample was made by measuring the sample moment as a function of temperature at both 3 and 4 T—i.e., in the linear region of the magnetization isotherm. Hysteresis measurements were made after cooling in the maximum field (5 T) and then measuring a full magnetization isotherm in the range ±5 T. Small corrections for core diamagnetism were carried out using standard tables.[44]

Electrical Conductivity Measurements. Rectangular bars of dimensions $5 \times 2 \times 1$ mm^3 were cut from sintered pellets of the materials used for the PND measurements. The resistivity was measured using the four-probe method with contacts made using silver-laden epoxy cement.

X-ray Absorption Near Edge Structure (XANES) Spectroscopy Measurements. Data were collected in transmission mode on station 7.1 of the Synchrotron Radiation Source, Daresbury Laboratory, UK. X-ray energies between 6.3 and 7.1 keV were selected using a Si(111) monochromator crystal and the position of the Mn K-edge at around 6.55 keV was measured for the oxysulfide samples and for binary and ternary standard materials. Each measurement was calibrated against a 5-μm thick manganese foil.

Results

Synthesis and Crystal Structures. $Sr_2MnO_2Cu_{1.5}S_2$. The $m = 1$ member of the series $Sr_2MnO_2Cu_{2m}S_{m+1}$ was reported as $Sr_2MnO_2Cu_2S_2$ following Rietveld analysis of PXRD data.[11] Our attempts to reproduce this composition revealed considerable copper deficiency in the oxysulfide (copper metal was observed on the surface of the pellets) similar to that in $Sr_4Mn_2O_4Cu_5S_5$.[10] Refinement against PND data of the structure of a sample made with composition "$Sr_2MnO_2Cu_2S_2$" produced a refined composition of $Sr_2MnO_2Cu_{1.48(1)}S_2$, and the relative phase fractions of this phase and surplus copper metal (the only

(35) Otwinowski, Z.; Minor, W. DENZO-SMN. In *Methods in Enzymology, Macromolecular Crystallography, Part A*; Carter, C. W., Jr., Sweets, R. M., Eds.; Academic Press: New York, 1997; Vol. 276.
(36) Sheldrick, G. M. *SHELX97*. Programs for Crystal Structure Analysis (Release 97-2); University of Göttingen: Germany, 1997.
(37) Farrugia, L. J. *J. Appl. Crystallogr.* **1999**, *32*, 837.
(38) The minimisation function was: $\sum w(|F_o|^2 - |F_c|^2)^2$, where $w \approx 1/[(\sigma(F_o))^2 + (aP)^2 + (bP)]$, $P \approx (|F_o|^2 + 2|F_c|^2)/3$. The details of the weighting scheme used in each case are given in the appropriate crystallographic information file.
(39) Wilson, A. J. C., Ed. *International Tables for Crystallography*, Volume C; Kluwer Academic Publishers: Dordrecht, The Netherlands, 1995.
(40) Alcock, N. W. *Cryst. Comput.* **1970**, 271.
(41) Spek, A. L. *Acta Crystallogr., Sect. A* **1990**, *46*, C34.
(42) LePage, Y. *J. Appl. Crystallogr.* **1987**, *20*, 264. Spek, A. L. *J. Appl. Crystallogr.* **1988**, *21*, 578.
(43) Larson, A.; von Dreele, R. B. *The General Structure Analysis System*; Los Alamos National Laboratory: Los Alamos, NM, 1985.
(44) *Landolt-Bornstein New Series II/10: Magnetic properties of transition metal compounds*; Springer-Verlag: Berlin, 1979; Supplement 2.

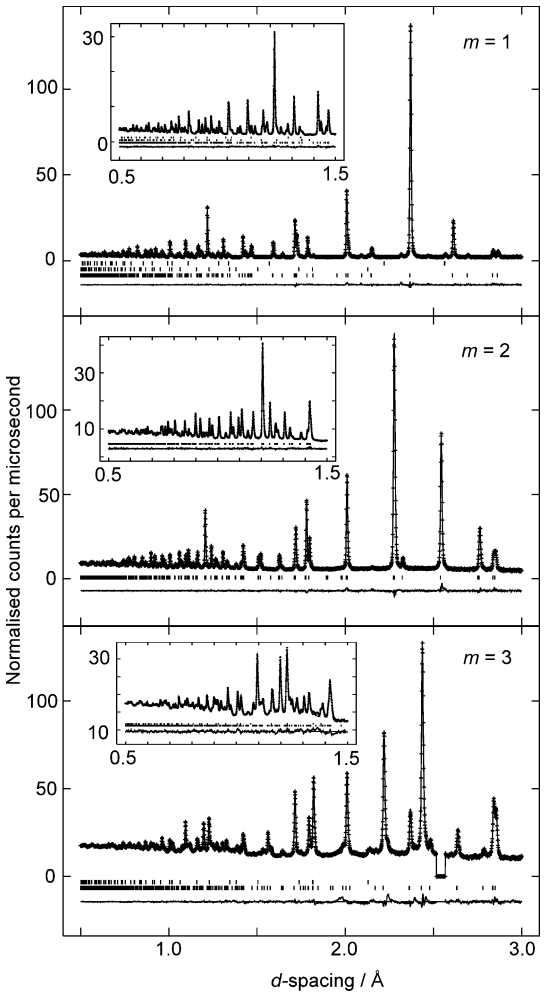

Figure 2. Refinements of $Sr_2MnO_2Cu_{1.5}S_2$ ($m = 1$, top), $Sr_2MnO_2Cu_{3.5}S_3$ ($m = 2$, middle), and $Sr_2MnO_2Cu_{5.5}S_4$ ($m = 3$, bottom) against POLARIS PND data (145° detector bank). The measured (points), calculated (line), and difference (lower line) profiles are shown. The lowest sets of tick-marks show allowed reflections for the main phases with refined compositions $Sr_2MnO_2Cu_{1.50(1)}S_2$, $Sr_2MnO_2Cu_{3.4(1)}S_3$, and $Sr_2MnO_2Cu_{5.5(2)}S_4$. 2% by mass SrS impurities in the $m = 1$ and $m = 3$ samples and a 0.5% by mass MnO impurity in the $m = 1$ sample (uppermost set of tick-marks) are included in the refinements. A weak reflection from an unidentified impurity phase was excluded from the $m = 3$ refinement. The insets show magnifications of the low *d*-spacing regions.

additional phase observed by PXRD measurements) were 2.1(1):1, consistent with the refined composition (i.e. independent refinements of the fractional occupancy of the copper site and the phase fraction of elemental copper in the sample produced consistent compositions for the oxysulfide phase). Refinement against data collected on a single crystal obtained from a sample synthesized at the composition suggested by the PND results yielded a refined composition of $Sr_2MnO_2Cu_{1.48(1)}S_2$—equal to within error of the composition obtained from the PND measurement. Subsequently, phase-pure (by PXRD) bulk material for property measurements was made on the 8-g scale by reacting together SrS, MnO_2, Mn, and CuO in the ratios 2:0.25:0.75:1.5 at 900 °C for 16 h. PND refinement on this sample (Figure 2) produced a refined composition of $Sr_2MnO_2Cu_{1.50(1)}S_2$. The results of refinement against SXRD and PND data are presented in Tables 1 and 2. The crystal structure derived from the SXRD refinement is shown in Figure 3. Preliminary electron diffraction measurements show a $2\sqrt{2}a \times \sqrt{2}a \times c$ expansion of the room-temperature unit cell at 110 K accompanied by twinning.

$Sr_2MnO_2Cu_{3.5}S_3$. The synthesis of $Sr_4Mn_2O_4Cu_5S_5$ with both "single"- and "double"-thickness antifluorite copper sulfide layers[10] suggested that $Sr_2MnO_2Cu_{4-\delta}S_3$ containing only "double" thickness layers might be attainable. A sample of composition "$Sr_2MnO_2Cu_4S_3$" prepared from SrS, Mn, CuO, and Cu_2S in the ratio 2:1:2:1 was heated at 900 °C for 13 days, and a sample of composition "$Sr_2MnO_2Cu_3S_3$" prepared from SrS, MnO_2, Cu_2S, and Cu in the ratio 2:1:1:1 was heated at 900 °C for 10 days. In the copper-rich case, excess copper metal had precipitated on the surface of the pellet. Small crystals were produced in the copper-poor reaction, and an SXRD study at 150 K after rapid cooling of the sample (i.e. in a few seconds) suggested a new compound crystallizing in *P*4/*mmm* with cell dimensions $a = 5.705$ Å, $c = 11.28$ Å, consistent with the expected dimensions for $Sr_2MnO_2Cu_{4-\delta}S_3$. Structure solution and refinement suggested the composition $Sr_2MnO_2Cu_{3.5}S_3$. Subsequently, single-phase powder samples for PND and physical property measurements were prepared at this composition on the 2−8-g scale from mixtures of SrS, MnO_2, Mn, CuO, and Cu_2S in the molar ratio 2:0.5:0.5:1.5:1 reacted together at 1000 °C for 18 h. The SXRD measurements reported here were made on crystals prepared by reaction at 900 °C carried out on the 2-g scale between SrO, Mn, Cu, and S in the ratio 2:1:3.5:3. EDX measurements on these crystals produced a Sr:Mn:Cu:S ratio of 1.7(1):1:3.4(1):2.9(1). SXRD measurements and PND measurements (Figure 2) showed that the room-temperature unit cell dimensions in space group *P*4/*mmm* were $a = 4.0217(1)$ Å and $b = 11.4180(3)$ Å (i.e. half the volume of the cell obtained after rapid cooling to 150 K). Electron diffraction measurements confirmed these dimensions (Figure 4). The crystal structure is shown in Figure 3.

The refined composition using SXRD was $Sr_2MnO_2Cu_{3.4(1)}S_3$. PND measurements on an 8-g sample prepared with the stoichiometry "$Sr_2MnO_2Cu_{3.5}S_3$" showed that this contained a single crystalline phase with a refined composition of $Sr_2MnO_2Cu_{3.4(1)}S_3$ when measured on POLARIS (Figure 2) and $Sr_2MnO_2Cu_{3.5(2)}S_3$ when measured on D2B. Compositions of $Sr_2MnO_2Cu_{3.6(1)}S_3$ and $Sr_2MnO_2Cu_{3.5(1)}S_3$ were obtained for further samples measured on POLARIS from starting materials which were slightly copper rich; in these cases the amount of elemental copper in the diffraction pattern accounted within error for the difference between the composition of the sample and the refined copper content in the oxysulfide phase. These values are all consistent with the EDX measurements. The reason for the relatively large uncertainty in the copper composition is that the copper atoms in the "double thickness" copper sulfide layers partially occupy several positions and have highly anisotropic displacement ellipsoids, as in $Sr_4Mn_2O_4Cu_5S_5$.[10] Our best description of the composition of this phase is $Sr_2MnO_2Cu_{3.5(2)}S_3$ based on the available independent measurements, consistent with the fact that the purest material is obtained when a composition of "$Sr_2MnO_2Cu_{3.5}S_3$" is used in synthesis. However, because of the experimental uncertainty in the determining the copper content, we cannot fully rule out the existence of a finite phase width in this compound. In the case of the $m = 1$ compound, $Sr_2MnO_2Cu_{1.5}S_2$, the uncertainty in the copper composition is much smaller because the copper ions occupy only one site in the "single" copper sulfide layers with much

Table 1. Results of Single Crystal X-ray Refinements for $Sr_2MnO_2Cu_{1.5}S_2$, $Sr_4Mn_2O_4Cu_5S_5$, $Sr_2MnO_2Cu_{3.5}S_3$, and $Sr_2MnO_2Cu_{5.5}S_4$

	$Sr_2MnO_2Cu_{1.5}S_2$	$Sr_4Mn_2O_4Cu_5S_5$	$Sr_2MnO_2Cu_{3.5}S_3$	$Sr_2MnO_2Cu_{5.5}S_4$	$Sr_2MnO_2Cu_{5.5}S_4$
refined composition	$Sr_2MnO_2Cu_{1.48(1)}S_2$	$Sr_4Mn_2O_4Cu_{5.0(1)}S_5$	$Sr_2MnO_2Cu_{3.4(1)}S_3$	$Sr_2MnO_2Cu_{5.2(3)}S_4$	$Sr_2MnO_2Cu_{5.5(3)}S_4$
radiation			Mo Kα, $\lambda = 0.71073$ Å		
instrument			Enraf Nonius FR590 κCCD		
physical form			black single crystal		
T/K	240(2)	293(2)	293(2)	293(2)	150(1)
space group	*I*4/*mmm*	*I*4/*mmm*	*P*4/*mmm*	*I*4/*mmm*	Cmca
formula weight	420.4(6)	1002(6)	574(6)	720(20)	740(20)
a/Å	4.0139(2)	4.0177(1)	4.0217(1)	4.0057(2)	28.214(2)
b/Å	*a*	*a*	*a*	*a*	5.6837(3)
c/Å	17.1663(9)	40.0019(9)	11.4180(3)	28.296(2)	5.6898(3)
V/Å^3	276.57(2)	645.71(3)	184.676(8)	454.03(4)	912.43(8)
Z	2	2	1	2	4
R1[a]	0.0202	0.0223	0.0213	0.0291	0.0637
wR2[a]	0.0387	0.0463	0.0407	0.0578	0.0850
GoF	1.225	1.037	1.1	1.128	1.072

[a] For all data.

Table 2. Results of PND Refinements at 295 K for $Sr_2MnO_2Cu_{1.5}S_2$, $Sr_2MnO_2Cu_{3.5}S_3$, and $Sr_2MnO_2Cu_{5.5}S_4$

	$Sr_2MnO_2Cu_{1.5}S_2$	$Sr_2MnO_2Cu_{3.5}S_3$	$Sr_2MnO_2Cu_{5.5}S_4$
refined composition	$Sr_2MnO_2Cu_{1.50(1)}S_2$	$Sr_2MnO_2Cu_{3.4(1)}S_3$	$Sr_2MnO_2Cu_{5.7(3)}S_4$
radiation		neutron	
instrument		POLARIS	
physical form		black powder	
T/K	295	295	295
space group	*I*4/*mmm*	*P*4/*mmm*	*I*4/*mmm*
Formula weight	420.4(6)	574(6)	750(20)
a/Å	4.01218(3)	4.01554(3)	4.01365(7)
c/Å	17.1916(2)	11.4052(1)	28.3917(6)
V/Å^3	276.743(5)	183.904(4)	457.37(1)
Z	2	1	2
R_{wp}	0.0237	0.0157	0.0139
R_{F2}	0.043	0.049	0.165
χ^2	2.076	1.246	2.336

smaller and almost isotropic displacement ellipsoids. While the cell suggested by SXRD for $Sr_2MnO_2Cu_{3.5}S_3$ after rapid cooling to 150 K was a $\sqrt{2}a \times \sqrt{2}a \times c$ expansion of the room temperature cell, measurements on crystals slowly cooled (at about 100 K per hour) below 190 K showed evidence for larger unit cell expansions. The nature of the supercells was investigated by electron diffraction measurements on the bulk sample for which PND and property measurements are reported. Three diffraction patterns all taken along the same direction, but under different conditions, and indexed on the tetragonal room-temperature cell for comparative purposes are shown in Figure 4, a−c. Figure 4a obtained at room temperature shows the same tetragonal cell (of dimensions a_T and c_T) as was determined from the SXRD and PND measurements (Tables 1 and 2). Figure 4b was obtained at 110 K from a different crystallite after rapid cooling (room temperature to 110 K in 30 min). The diffractogram shown in Figure 4c was obtained from the same crystallite as that shown in 4a after slow cooling (i.e., 100 K per hour, as for the SXRD measurements).[45]

The measurement carried out with rapid cooling suggested an incommensurate modulation with an approximately $4\sqrt{2}a_T \times 4\sqrt{2}a_T$ basal expansion of the room-temperature tetragonal cell. The measurements carried out after slow cooling showed a 12-fold volume expansion of the room-temperature tetragonal cell, yielding a monoclinic supercell with dimensions $a = 9.1$ Å ($\sqrt{5}a_T$), $b = 23.2$ Å ($2c_T$), $c = 11.4$ Å ($2\sqrt{2}a_T$), and $\beta = 109°$ and real space unit cell vectors obtained by multiplying the tetragonal cell vectors by the matrix

$$\begin{bmatrix} 2 & 1 & 0 \\ -2 & 2 & 0 \\ 0 & 0 & 2 \end{bmatrix}$$

The systematic absences were consistent only with space group $P2_1/c$. The diffraction patterns along the main directions for the monoclinic phase are shown in Figure 4, d− f. The presence on the [100] diffraction pattern of the 00*l*: $l = 2n + 1$ reflections, forbidden for $P2_1/c$, is due to double diffraction: verified by their absence on [010]. The 0*k*0: $k = 2n + 1$ reflections, present on [100] and [010], are also due to double diffraction: verified by tilting the crystallites around the *b** axis, resulting in the disappearance of these reflections. Further investigations of the low-temperature structures are in progress.

$Sr_2MnO_2Cu_{5.5}S_4$. Evidence for $Sr_2MnO_2Cu_{6-\delta}S_4$, the $m =$ 3-member of the homologous series $Sr_2MnO_2Cu_{2m}S_{m+1}$, was first found from black crystals grown in a pellet of composition "$LaSr_3Mn_3Cu_4O_{7.5}S_3$". The unit cell was determined to be tetragonal with lattice parameters $a = 4.02$ Å and $c = 28.2$ Å, and the systematic absences were consistent with a body-centered lattice. Structure solution in space group *I*4/*mmm* yielded the structure of the $m = 3$-member of the homologous series $Sr_2MnO_2Cu_{2m-\delta}S_{m+1}$. A sample of composition "$Sr_2MnO_2Cu_5S_4$", prepared from a 2:1:2:1 mixture of SrS, MnO_2, Cu_2S, and Cu heated at 900 °C for 10 days and cooled at 0.1 °C min^{-1}, yielded crystals and powder of $Sr_2MnO_2Cu_{6-\delta}S_4$ as

(45) Diffractogram 4 (c) was recorded first, and the sample was then warmed prior to measurement of diffractogram 4 (a).

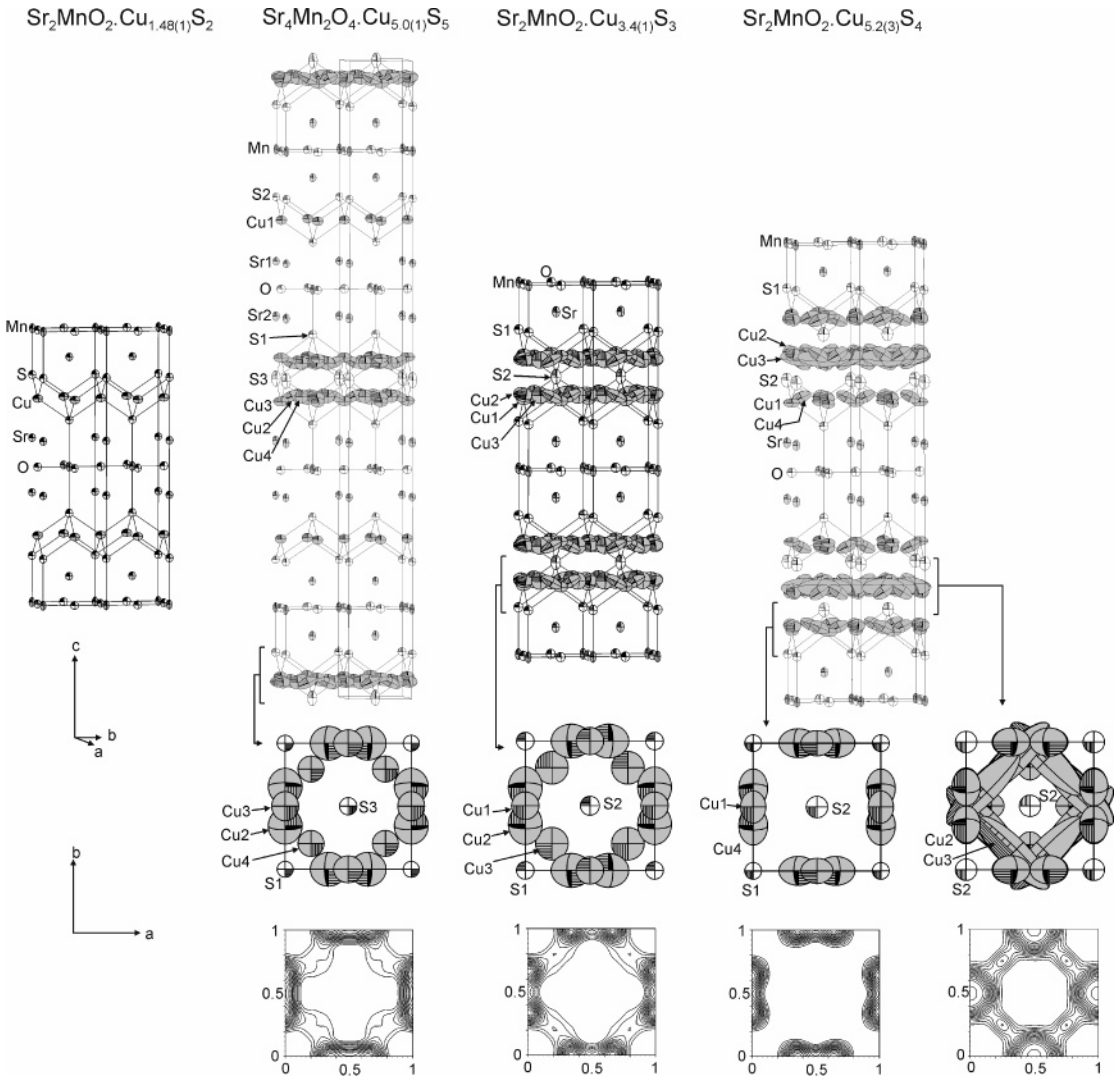

Figure 3. The room-temperature structures of $Sr_2MnO_2Cu_{1.5}S_2$, $Sr_4Mn_2O_4Cu_5S_5$, $Sr_2MnO_2Cu_{3.5}S_3$, and $Sr_2MnO_2Cu_{5.5}S_4$ derived from refinement against SXRD data; 75% displacement ellipsoids are shown. The bottom series of diagrams shows the observed Fourier map of the electron density due to copper in each of the disordered layers.

the majority product. SXRD measurements on the crystals produced by these methods suggested the composition was close to $Sr_2MnO_2Cu_{5.5}S_4$ and showed that the copper ions in the copper sulfide layers were extremely delocalized. The highest-quality single crystals were prepared using a KI flux: SrS, MnO_2, Mn, CuO, and Cu_2S were mixed in the molar ratio 8:1:3:6:4, and 0.25 g of this mixture was ground with 0.196 g of KI, and the mixture was reacted as described in the Experimental Section. EDX measurements on crystals so produced revealed a Sr:Mn:Cu:S ratio of 1.8(1):1:5.0(1):3.9(1). The refined composition of such crystals from SXRD analysis at room temperature was $Sr_2MnO_2Cu_{5.2(3)}S_4$, and the results of the refinement are presented in Table 1; the structure is shown in Figure 3. A bulk powder sample (2 g in mass) with this composition was prepared by reacting together a well-ground pelletized mixture of SrS, MnO_2, Cu_2S, and Cu in the molar ratio 2:1:1:1.2 at 850 °C for 18 h. The results of Rietveld refinement against POLARIS data obtained on this sample, which contains a small SrS impurity, are shown in Figure 2. The PND refinement suggested a slightly higher copper content (refined composition $Sr_2MnO_2Cu_{5.7(2)}S_4$) than that obtained from the room-temperature refinement against SXRD data collected on the flux-grown crystals ($Sr_2MnO_2Cu_{5.2(2)}S_4$), although the values are equal within 3σ. Attempts to synthesize bulk powder materials with compositions ranging between "$Sr_2MnO_2Cu_{5.2}S_4$" and "$Sr_2MnO_2Cu_{5.5}S_4$" invariably produced samples which contained some small amounts of SrS and other unidentified phases. Reaction temperatures above 850 °C, longer heating times, and repeated grinding and heating cycles were found to lead to degradation of the sample with the formation of $Sr_2MnO_2Cu_{3.5}S_3$ as a notable side product. The refined compositions from the room-temperature SXRD study ($Sr_2MnO_2Cu_{5.2(2)}S_4$), and PND investigations of different bulk powders on POLARIS ($Sr_2MnO_2Cu_{5.7(2)}S_4$) and D2B ($Sr_2MnO_2Cu_{5.7(2)}S_4$ and $Sr_2MnO_2Cu_{5.6(3)}S_4$) together with the EDX study ($Sr_2MnO_2Cu_{5.1(4))}S_4$) suggest that a composition of $Sr_2MnO_2Cu_{5.5(3)}S_4$ is reasonable. The large uncertainty is, as in $Sr_2MnO_2Cu_{3.5}S_3$, due to the delocalized nature of the copper ions in the copper sulfide layers, and we cannot yet rule out the existence of a finite phase width in this compound.

Slow cooling of a crystal to 150 K on the diffractometer yielded a diffraction pattern for which the highest Laue symmetry compatible with the cell metrics was orthorhombic *mmm* (R_{merge}[46] = 0.069 compared with R_{merge} = 0.232 (4/*m*) or

Table 3. Metal−Anion Bond Distances in Å for the Four Compounds Obtained from SXRD Measurements at Room Temperature

	bond length/Å			
bond	$Sr_2MnO_2Cu_{1.5}S_2$	$Sr_4Mn_2O_4Cu_5S_5$	$Sr_2MnO_2Cu_{3.5}S_3$	$Sr_2MnO_2Cu_{5.5}S_4$
Mn−O [4][a,b]	2.0070(1)	2.0094(1)	2.0076(1)	2.0029(1)
Mn−S [2]	2.915(1)	2.804(1)/2.986(1)	2.877(1)	2.835(1)
Sr−O [4]	2.6372(3)	2.612(1) (Sr(1)−O) 2.679(1) (Sr(2)−O)	2.6463(4)	2.6607(3)
Sr−S [4]	3.0833(6)	3.1117(4) (Sr(1)−S(2)) 3.0391(4) (Sr(2)−S(1))	3.0645(5) (Sr−S(1))	3.0324(5) (Sr−S(1))
$Cu-S_{single}$ [4][c]	2.4335(7)	2.4398(5) (Cu(1)−S(2))		
$\langle Cu-S\rangle_{outer}$ [4][d]		2.456	2.459	2.441
$\langle Cu-S\rangle_{inner}$ [4][d]				2.474

[a] The numbers in square brackets indicate the number of bonds of a particular type. [b] The Mn−O distances in each case are equal to half the basal lattice parameter. [c] $Cu-S_{single}$ signifies the Cu−S distance in a "single" thickness $Cu_{2-\delta}S_2$ layer. [d] The ⟨Cu−S⟩ distances are calculated assuming an idealized location of a copper ion in the center of a distorted tetrahedron described by four sulfur atoms. $\langle Cu-S\rangle_{outer}$ indicates the distance in the outer S−Cu−S layers in the thicker copper sulfide slabs, and $\langle Cu-S\rangle_{inner}$ indicates the distance in the central part of the copper sulfide slab in $Sr_2MnO_2Cu_{5.5}S_4$.

$R_{merge} = 0.236$ (4/*mmm*) for tetragonal symmetry). A satisfactory structure solution was obtained in space group *Cmca* with the lattice parameters $a = 28.214(2)$ Å, $b = 5.6837(3)$ Å, $c = 5.6898(3)$ Å at 150 K, and $Z = 4$ (Table 1). The locations of the copper ions were determined from the Fourier difference map. The refined composition from this low-temperature SXRD investigation was $Sr_2MnO_2Cu_{5.5(3)}S_4$—slightly higher than that obtained in the room-temperature SXRD measurement on the same crystal. Preliminary investigation of the system using electron diffraction suggests that a more complex superstructure is obtained at 100 K, but correct indexing is hampered by twinning.

$Sr_4Mn_2O_4Cu_5S_5$. We have previously reported[10] the structure of this 1:1 intergrowth of the $m = 1$ and $m = 2$ members of the $Sr_2MnO_2Cu_{2m}S_{m+1}$ series. Higher-quality single crystals were prepared by reacting together SrS, MnO_2, Mn, and CuO in the molar ratio 8:1:3:6 at 900 °C and then recrystallizing 0.235 g of the resulting product with 0.265 g of KI flux. EDX measurements on these crystals produced a Sr:Mn:Cu:S ratio of 1.8(1):1:2.4(1):2.6(1), consistent with the refined composition of $Sr_4Mn_2O_4Cu_{5.0(1)}S_5$. The results of the refinement are listed in Table 1. The structure is shown in Figure 3.

Comparison of Crystal Structures. The geometries of the Sr_2MnO_2 cationic layers are very similar in all four compounds. Mn is in square planar coordination by four oxide ions forming MnO_2 sheets, and is additionally weakly coordinated axially by two sulfide ions. The Mn−O and Mn−S distances are summarized in Table 3. The main difference between the compounds is in the nature of the copper sulfide layers. In our report of $Sr_4Mn_2O_4Cu_5S_5$[10] we described $Cu_{2-\delta}S_2$ "single" layers with well-localized copper ions and $Cu_{4-\delta}S_3$ "double" layers with highly disordered copper ions; these were modeled using partial occupancy of the ideal tetrahedral site and partial occupancy of trigonal sites directed toward the two faces of CuS_4 tetrahedra which pointed toward the center of the layers. In this respect the $Cu_{4-\delta}S_3$ "double" layers resemble fragments of the α-Cu_2S fast-ion conducting phase.[47] Our analysis of $Sr_2MnO_2Cu_{4-\delta}S_3$ and $Sr_2MnO_2Cu_{6-\delta}S_4$, containing only "double"- and "triple"-thickness copper sulfide layers respectively shows that the copper ion disorder in the thicker layers is the norm. In the SXRD refinements we modeled the copper scattering density using up to four crystallographic sites until the difference Fourier map indicated that all the scattering density was accounted for in the model. Inevitably this approach to accounting for the smeared out scattering density leads to reasonably large errors in the refined copper contents of these phases as discussed above. The use of a KI flux for crystal growth produced higher-quality crystals of $Sr_4Mn_2O_4Cu_5S_5$ than we reported previously,[10] and additional copper density in $Sr_4Mn_2O_4Cu_5S_5$ (site Cu(4)) was consistently located in analysis of the diffraction patterns of the flux-grown crystals. This site corresponds to the site Cu(3) located in similar "double" thickness copper sulfide layers in the structure of $Sr_2MnO_2Cu_{3.5}S_3$. Figure 3 shows the refined structures from SXRD measurements for all four phases including observed Fourier maps of the electron density due to copper ions in $Sr_2MnO_2Cu_{3.5}S_3$, $Sr_2MnO_2Cu_{5.5}S_4$, and $Sr_4Mn_2O_4Cu_5S_5$. The PND refinements gave entirely consistent results. The relationship between the crystallographic disorder and the structural parameters is discussed below.

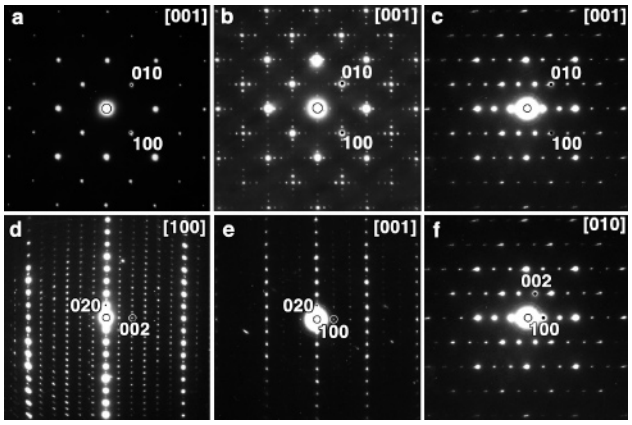

Figure 4. Electron diffraction patterns of $Sr_2MnO_2Cu_{3.5}S_3$. Room-temperature diffractogram (a) confirms the tetragonal cell (Tables 1 and 2). Diffractogram (b), measured at 110 K after rapid cooling from room temperature, shows an incommensurate modulation with an approximately $4\sqrt{2}a \times 4\sqrt{2}a$ basal expansion of the room-temperature tetragonal cell. Diffractogram (c), measured at 110 K after slow cooling of the sample from room temperature, shows a monoclinic cell 12 times the volume of the room-temperature cell. Diffractograms (a), (b), and (c) are indexed according to the room-temperature cell. Diffractograms (d), (e), and (f), the 110 K diffraction patterns measured along the three main zones of the same phase as measured in (c), are indexed on the monoclinic cell. (c) and (f) show the same diffractogram indexed on the tetragonal (c) and monoclinic (f) cells.

Magnetic Susceptibility Measurements. Figure 5 shows the magnetic susceptibilities measured as functions of temperature of the samples of $Sr_2MnO_2Cu_{1.5}S_2$, $Sr_2MnO_2Cu_{3.5}S_3$, and Sr_2-

(46) $R_{merge} = \sum [|(F^2(obs) - F^2(mean))|]/\sum[F^2(obs)]$.
(47) Oliveria, M.; McMullan, R. K.; Wuensch, B. J. *Solid State Ionics* **1988**, *28−30*, 1332.

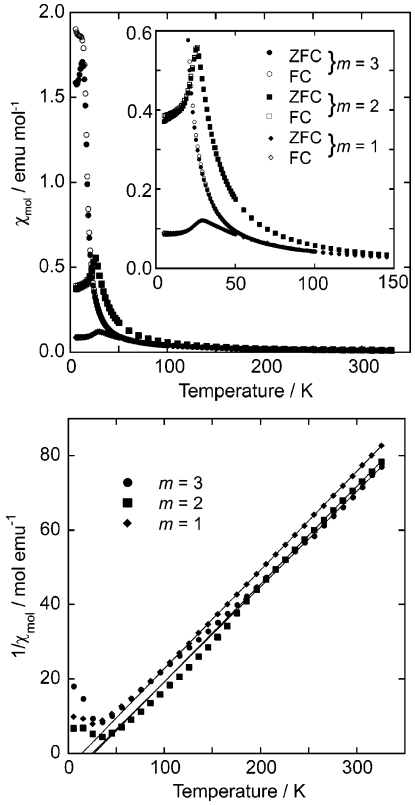

Figure 5. (Top) Magnetic susceptibilities of $Sr_2MnO_2Cu_{2m-\delta}S_{m+1}$ measured in a field of 100 mT after cooling in zero field (filled symbols) and in the measuring field (open symbols): $Sr_2MnO_2Cu_{1.5}S_2$ ($m = 1$; ◆, ◇), $Sr_2MnO_2Cu_{3.5}S_3$ ($m = 2$; ■, □), and $Sr_2MnO_2Cu_{5.5}S_4$ ($m = 3$; ●, ○). (Bottom) Inverse magnetic susceptibilities of $Sr_2MnO_2Cu_{1.5}S_2$ (◆), $Sr_2MnO_2Cu_{3.5}S_3$, (■), and $Sr_2MnO_2Cu_{5.5}S_4$ (●). The lines are extrapolations of fits[48] to the linear regions above 200 K which produced the parameters given in the text.

$MnO_2Cu_{5.5}S_4$ used for PND investigations. The measurements show that between 200 and 300 K these samples all obey the Curie−Weiss law.[48] The Curie constant for several samples of $Sr_2MnO_2Cu_{1.5}S_2$ is fairly consistent with that reported[11] for material with a reported composition of $Sr_2MnO_2Cu_2S_2$ (i.e. reportedly not copper deficient). An effective magnetic moment (μ_{eff}) of 5.3 μ_B per manganese ion was reported,[11] significantly lower than the spin-only μ_{eff} of 5.92 μ_B expected for the high-spin d^5 configuration of Mn^{2+}. Our mean μ_{eff} for three samples of $Sr_2MnO_2Cu_{1.5}S_2$ is determined to be 5.45(3) μ_B, consistent with the previous report and similar to the value of 5.43 μ_B expected for a mean Mn oxidation state of +2.5. $Sr_2MnO_2Cu_{3.5}S_3$ (μ_{eff} = 5.55(2) μ_B) and $Sr_2MnO_2Cu_{5.5}S_4$ (mean μ_{eff} = 5.28(5) μ_B) yield similar effective moments. The positive Weiss constants for $Sr_2MnO_2Cu_{1.5}S_2$ (+16(2) K), $Sr_2MnO_2Cu_{3.5}S_3$ (+27(2) K), and $Sr_2MnO_2Cu_{5.5}S_4$ (+24(3) K) contrast with the negative value reported previously for $Sr_2MnO_2Cu_2S_2$[11] and suggest that the dominant exchange interactions in the temperature range 200−300 K are ferromagnetic.

Low-temperature magnetic susceptibility measurements in measuring fields of 0.1 T or less show evidence for antiferromagnetic ordering in $Sr_2MnO_2Cu_{1.5}S_2$ ($m = 1$) and $Sr_2MnO_2Cu_{3.5}S_3$ ($m = 2$) at 29 and 26 K respectively. The observation for the $m = 1$ member is consistent with previous observations.[11] $Sr_2MnO_2Cu_{5.5}S_4$ ($m = 3$) shows evidence for ferromagnetic ordering of the manganese moments when measured in a field of 0.1 T. Magnetization isotherms measured at 5 K (Figure 6) show that the $m = 3$ compound is ferromagnetic with a moment of 3.2 μ_B per manganese ion in an applied field of 5 T which appears to be close to the saturation regime. This value approaches the value expected for full ferromagnetic ordering of all the manganese moments. The $m = 2$ compound is driven into the ferromagnetic regime by the application of a magnetic field exceeding 1.3 T, and the saturation moment is comparable to the value obtained in the $m = 3$ compound. The magnetization isotherm for the $m = 2$ compound exhibits a pronounced hysteresis which is under investigation. The $m = 1$ compound does not enter the ferromagnetic regime at magnetic fields of up to 7 T, but there is an upturn in the magnetization at the high-field region of the isotherm which suggests that this compound may become ferromagnetic at higher fields.

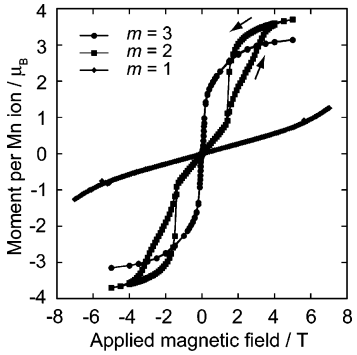

Figure 6. Magnetic moments per Mn ion of $Sr_2MnO_2Cu_{1.5}S_2$ (◆), $Sr_2MnO_2Cu_{3.5}S_3$ (■), and $Sr_2MnO_2Cu_{5.5}S_4$ (●) as a function of applied field measured at 5 K. The lines are guides to the eye.

Magnetic Neutron Scattering. A sample of $Sr_2MnO_2Cu_{5.5}S_4$ was cooled to 5 K in zero applied field on D2B. New reflections at low scattering angles were observed which could be indexed on a primitive orthorhombic cell with lattice parameters a = 28.161(2) Å, b = 5.6698(6) Å, and c = 5.6864(6) Å, i.e., with the same volume as the *C*-centered cell describing the 150 K crystal structure. The intensity of these new reflections was modeled using an *A*-type antiferromagnetic arrangement of manganese moments of 3.4(2) μ_B in which the identical moments in each of the MnO_2 planes were arranged ferromagnetically and aligned along the [1 0 0] direction of the cell of the orthorhombic 150 K model (i.e. the moments are directed perpendicular to the MnO_2 planes). The moments in neighboring planes were aligned antiferromagnetically. Alternative antiferromagnetic models and moment directions did not account for the observed scattering. In a vertical magnetic field of 5 T applied at 5 K the zero-field magnetic reflections had zero observable intensity, while the nuclear Bragg peaks at low scattering angle were enhanced in intensity. On warming from 5 to 75 K in the applied field of 5 T the intensity of these reflections diminished. The additional intensity at 5 K was modeled using a ferromagnetic alignment of all the manganese moments with refined moments of 4.6(2) μ_B aligned in the *ac* plane at an angle of 55(1)° to the MnO_2 planes. These refinements (Figure 7) were hampered by the observation that the 150 K structural model which was used is not adequate at temperatures below 100 K. A qualitatively similar evolution of the magnetic scattering is observed for $Sr_2MnO_2Cu_{3.5}S_3$. However, in this case the measurements carried out in an applied field were complicated by field-induced preferred orientation

(48) The susceptibility was fit to $\chi = C/(T - \theta)$ in the temperature range 200 K < T < 300 K.

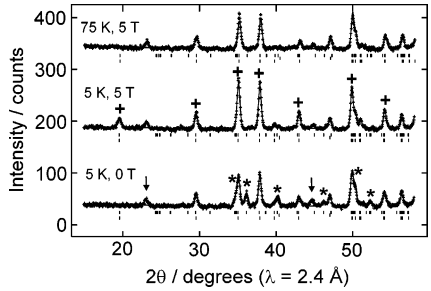

Figure 7. Refinement of the magnetic structures of $Sr_2MnO_2Cu_{5.5}S_4$ against D2B data ($\lambda = 2.4$ Å). In zero applied field (bottom) *A*-type antiferromagnetic ordering is adopted. In a 5 T magnetic field (middle) Bragg scattering resulting from antiferromagnetic ordering (*) is replaced by Bragg scattering resulting from ferromagnetic ordering which enhances nuclear Bragg intensities (+). At 75 K the magnetic scattering is almost zero (top). The measured (points) and fit (line) are shown with tick marks for the *C*-centered orthorhombic nuclear cell (lower), a small amount of SrS impurity (middle), and the primitive magnetic cell with the same volume as the nuclear cell (upper). Two unidentified reflections (↓) arise either from magnetic Bragg scattering from an impurity phase or from an unresolved low-temperature expansion of the nuclear cell. The diffractograms are shown on the same scale but are offset relative to one another by 150 counts along the vertical axis.

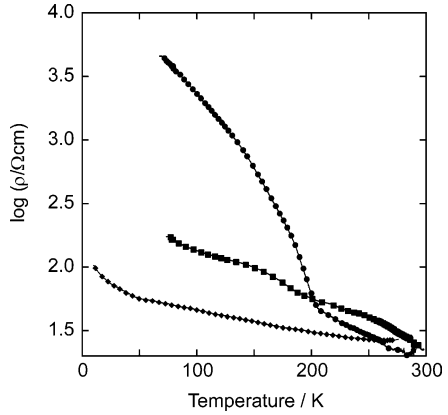

Figure 8. Electrical resistivity as a function of temperature for the samples of $Sr_2MnO_2Cu_{1.5}S_2$ (◆), $Sr_2MnO_2Cu_{3.5}S_3$ (■), and $Sr_2MnO_2Cu_{5.5}S_4$ (●) used in the PND experiments.

and by the complex structural changes evident from the low-temperature electron diffraction measurements. Further neutron diffraction measurements on powder and single-crystal samples coupled with the results of low-temperature electron diffraction measurements are required to resolve the low-temperature crystal and magnetic structures of these compounds.

Transport Measurements. Measurement of the electrical resistivities of $Sr_2MnO_2Cu_{1.5}S_2$, $Sr_2MnO_2Cu_{3.5}S_3$, and $Sr_2MnO_2Cu_{5.5}S_4$ (Figure 8) showed that all three materials are semiconducting. The resistivities increase on cooling from room-temperature values of 27(1) Ω cm for $Sr_2MnO_2Cu_{1.5}S_2$, 20(1) Ω cm for $Sr_2MnO_2Cu_{3.5}S_3$, and 24(1) Ω cm for $Sr_2MnO_2Cu_{5.5}S_4$. The resistivity of $Sr_2MnO_2Cu_{5.5}S_4$ shows a sharp change in the gradient at 210 K presumably associated with the structural changes described above. The resistivity of $Sr_2MnO_2Cu_{3.5}S_3$ shows less dramatic changes in gradient which may also be associated with the complex structural changes observed in that compound. The Seebeck coefficient measured at room temperature for a sample of $Sr_2MnO_2Cu_{3.5}S_3$ was positive in sign indicating majority hole carriers.

XANES Measurements. XANES measurements (Figure 9) show a spread of absorption edges for $Sr_2MnO_2Cu_{1.5}S_2$, $Sr_2MnO_2Cu_{3.5}S_3$, and $Sr_2MnO_2Cu_{5.5}S_4$ of only 0.6 eV, suggesting that the Mn oxidation states are very similar in the three members of the series. The positions of the absorption edges suggest that, even allowing for the different coordination geometries, the Mn oxidation state in the oxysulfides is intermediate between those in MnO and Mn_2O_3.

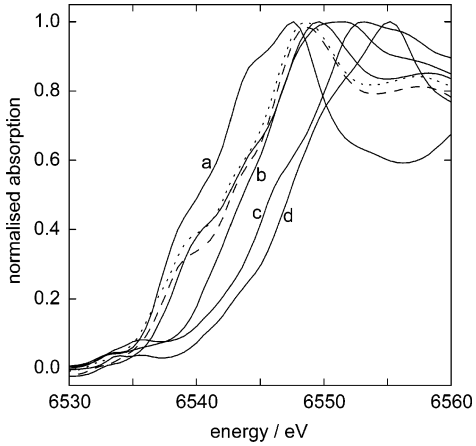

Figure 9. Mn K-edge XANES spectra for $Sr_2MnO_2Cu_{1.5}S_2$ (dotted line), $Sr_2MnO_2Cu_{3.5}S_3$ (dashed line), and $Sr_2MnO_2Cu_{5.5}S_4$ (solid line) compared with the spectra for MnO (a), Mn_2O_3 (b), MnO_2 (c), and $CaMnO_3$ perovskite (d).

Discussion

Composition, Structures, and Electronic Properties. The four members of the $Sr_2MnO_2Cu_{2m-\delta}S_{m+1}$ series ($m = 1$, 2, 3 and the intergrowth of the $m = 1$ and $m = 2$ members which has an effective m of 1.5) have similar copper deficiencies per Mn ion with $\delta \approx 0.5$ indicated by the compositions required to synthesize single-phase samples and from the SXRD and PND refinements. The refined Mn−O distances in the four compounds cover a range 2.006 ± 0.003 Å at room temperature, i.e., the greatest difference in analogous distances is 0.3% and the Mn−S distances range between 2.835(1) Å in $Sr_2MnO_2Cu_{5.5}S_4$ and 2.922(1) Å in $Sr_2MnO_2Cu_{1.5}S_2$. This alone suggests that the Mn oxidation states in the four compounds are all very similar. The narrow spread of absorption edge energies of 0.6 eV in the XANES experiment and the similar effective magnetic moments per Mn ion obtained from magnetic susceptibility measurements support this conclusion.

The compounds $ACu_{2m}S_{m+1}$ (A = Tl for $m = 1$, 3; A = Tl, K, Rb, Cs for $m = 2$) contain similar copper sulfide layers to those reported here. Since A forms a monovalent cation, the formulation of the copper sulfide layers is $[Cu_{2m}S_{m+1}]^-$. Since copper has only been observed in the monovalent state in copper chalcogenides, this is interpreted as one hole per formula unit at the top of the valence band. The $Cu_{2m}S_{m+1}$ layers readily accommodate holes because the Cu−S, Cu−Cu, and S−S antibonding crystal orbitals which lie at the top of the valence band are readily depleted.[33,50] The metallic properties measured in the series $TlCu_{2m}S_{m+1}$[25,27] and KCu_4S_3[29] demonstrate that the holes are mobile, in accord with the large calculated Cu-3*d*/S-3*p* overlaps for the hole states.[33]

One rationalization, therefore, of the copper deficiencies of the manganese oxysulfides reported here is that in each case

(49) Brese, N. E.; O'Keeffe, M. *Acta Crystallogr., Sect. B: Struct. Sci.* **1991**, *47*, 192.
(50) Berger, R.; van Bruggen, C. F. *J. Less Common Metals* **1985**, *113*, 291.

there are δ ($\sim$0.5) holes in the valence band per $Sr_2MnO_2Cu_{2m-\delta}S_{m+1}$ formula unit and the oxidation state of Mn is +2. However, the values of the effective moments per Mn ion suggest that Mn is oxidized to approximately the +2.5 oxidation state. Bond valence calculations[49] support this, producing values of 2.51 ($m = 1$), 2.53 ($m = 1/m = 2$ intergrowth), 2.55 ($m = 2$), and 2.61 ($m = 3$). Furthermore, the XANES measurements (Figure 9) suggest, even allowing for the different coordination geometries, a Mn oxidation state intermediate between those in MnO and Mn_2O_3. Apart from these direct measurements of the Mn oxidation state, the semiconducting nature of $Sr_2MnO_2Cu_{1.5}S_2$, $Sr_2MnO_2Cu_{3.5}S_3$, and $Sr_2MnO_2Cu_{5.5}S_4$ provides further evidence that, unlike the metallic $TlCu_{2m}S_{m+1}$ series[25,27,28] and KCu_4S_3,[29] the Cu-3*d*/S-3*p* valence band is full, and therefore manganese is oxidized. Calculations on the copper sulfide layers[33] suggest that in the compounds reported here S-3p_x/p_y orbitals can overlap in a π-sense with the Mn-3d_{xz}/d_{yz} orbitals and S-3p_z can overlap in a σ-sense with the Mn-3d_{z^2} orbital. Such overlap will stabilize the Cu-3*d*/S-3*p* antibonding states at the top of the valence band at the expense of the Mn-based states, which will become more antibonding. Thus, the antibonding Cu-3*d*/S-3*p* states may formally be filled by oxidation of the manganese ions. A rationalization of this is that the copper deficiency is the variable which allows optimization of the electron count in response to the interaction between the oxide and sulfide layers.

Magnetic Ordering. The PND and magnetometry measurements show that in zero or very low applied magnetic fields these compounds exhibit *A*-type antiferromagnetic ordering below about 30 K with ferromagnetic sheets coupled antiferromagnetically. In sufficiently large applied magnetic fields, the antiferromagnetic coupling between the sheets is overcome, and the $m = 2$ and $m = 3$ compounds exhibit close to full ferromagnetic ordering in 5 T fields. The between-plane coupling decreases in strength as the thickness of the copper sulfide layers increases and is therefore overcome by fields as low as 0.06 T in the $m = 3$ compound, but is not overcome at routinely attainable fields in the $m = 1$ compound.

The explanation for the in-plane ferromagnetism is unclear. At room temperature there is only one crystallographically unique Mn ion with a mean oxidation state of approximately +2.5. At low temperatures the superstructures suggested by electron diffraction measurements are complex and, at least in the $m = 2$ case, dependent on the thermal history of the sample. We are as yet unable to refine the low-temperature crystal structures with any certainty because the large supercells require an unacceptably large number of structural variables to be refined. For Mn^{2+} and Mn^{3+} ions in sites with 4/*mmm* symmetry the dominant 180° σ-type superexchange interaction involving the $d_{x^2-y^2}$ orbitals on Mn and mediated by the O-2$p_{x,y}$ orbitals is expected to be antiferromagnetic between pairs of Mn^{2+} or Mn^{3+} ions, but to be ferromagnetic between a Mn^{2+} ion and a Mn^{3+} ion. Therefore, low-temperature charge ordering between the equal populations of distinct Mn^{2+} and Mn^{3+} centers in the MnO_2 sheets should result in ferromagnetic sheets. However, while the low-temperature structural distortions are of the type that could enable low-temperature charge-ordering to occur, or may be driven by it, there is no direct evidence for charge ordering. Indeed the orthorhombic structure reported here of $Sr_2MnO_2Cu_{5.5}S_4$ at 150 K still contains only one crystallographically unique Mn site. An alternative explanation for the ferromagnetism of the sheets might be that the Mn ions are coupled ferromagnetically via double exchange involving itinerant Mn-3$d_{x^2-y^2}$ electrons. This should result in materials that are metallic in two dimensions which is not evident from our conductivity measurements on powder samples. The relationship between the crystal structures and the magnetic properties and the possibility of enhancements in the electrical conductivity in the ferromagnetic state, comparable with those observed in mixed-valent $3d^3/3d^4$ ternary manganese oxides, are currently under investigation using further electron diffraction measurements, and using further PND and transport measurements in applied magnetic fields.

Copper Ion Disorder and Mobility. The room-temperature crystal structures of the $Sr_2MnO_2Cu_{2m-\delta}S_{m+1}$ series show that the copper vacancies are disordered, and in the $m = 2$ and $m = 3$ compounds there is further copper site disorder. In contrast, in the $TlCu_{2m}S_{m+1}$ analogues the copper ion displacement ellipsoids are not unusually large. In the $TlCu_{2m}S_{m+1}$ series the basal lattice parameters which correspond to the length of one edge of a CuS_4 tetrahedron increase with *m* from 3.7771(1) Å in $TlCu_2S_2$ ($m = 1$) to 3.9357(5) Å in $TlCu_{5.5}S_4$ ($m = 3$).[33] The interlayer S−S distances, corresponding to the other crystallographically distinct edges of the CuS_4 tetrahedra, decrease as *m* increases with the mean Cu−S distance of 2.40 Å remaining approximately constant with *m*. This squashing of the CuS_4 tetrahedra along the direction perpendicular to the layers as *m* increases, is presumably dictated by the precise nature of the band structure in the $TlCu_{2m}S_{m+1}$ series. In our $Sr_2MnO_2Cu_{2m-\delta}S_{m+1}$ series the rigid $[Sr_2MnO_2]^{(2+\delta)+}$ layers fix the basal lattice parameters and therefore the in-plane S−S edge of a CuS_4 tetrahedron. The interlayer S−S distances are observed to *increase* from 3.9674 Å in $Sr_2MnO_2Cu_{1.5}S_2$ to 4.0544 Å in the central part of the copper sulfide layer in $Sr_2MnO_2Cu_{5.5}S_4$. This is presumably dictated by the filling of S−S antibonding states near the top of the valence band.[50] The consequence of this is that, unlike in the $TlCu_{2m}S_{m+1}$ series, the size of the CuS_4 tetrahedral site increases with increasing *m*. This is summarized in Table 3 which gives the mean distances from the sulfur atoms to the centers of the tetrahedral sites for each type of layer. The response of the copper ions is to move away from the centers of the tetrahedra to mainly occupy less highly coordinated trigonal sites located toward the faces of the tetrahedral sites. The degree of delocalization of the copper ions correlates extremely closely with the size of the tetrahedral site. Figure 3 shows that for the outer site in the $Cu_{5.5}S_4$ "triple" layer the scattering density is less delocalized than in the similar sites in the two $Cu_{3.5}S_3$ "double" layers found in $Sr_2MnO_2Cu_{3.5}S_3$ and $Sr_4Mn_2O_4Cu_5S_5$ and this accords with the slightly larger sites in the two "double" layers. The CuS_4 tetrahedron in the center of the $Cu_{5.5}S_4$ layer in $Sr_2MnO_2Cu_{5.5}S_4$ has the largest mean Cu−S distance, and accordingly, the copper scattering density is extremely delocalized with very little residing at the center of the S_4 tetrahedron as shown in Figure 3. While the copper ions are disordered at room temperature according to our X-ray, neutron, and electron diffraction measurements, long-range ordering of the copper ions and copper ion vacancies may be the driving force for the low-temperature structural distortions. The copper sulfide slabs in these compounds resemble fragments of the α-Cu_2S fast ion-conducting phase, and the delocalized

nature of the copper scattering density suggests high copper ion mobility. Recent investigations show that the copper ions in $Sr_2MnO_2Cu_{1.5}S_2$, $Sr_2MnO_2Cu_{3.5}S_3$, and $Sr_2MnO_2Cu_{5.5}S_4$ are chemically exchangeable at room temperature by lithium ions,[51] suggestive of high mobility.

Conclusions

We have synthesized several members of an homologous series of layered transition metal oxysulfides. Although these contain well-defined distinct metal oxide and metal sulfide layers according to the chemical preferences of the metals, we have shown that the compositions, structures, and electronic and magnetic properties of these compounds are determined by the interaction between the oxide and chalcogenide layers. Compounds containing the thinnest copper sulfide layers are numerous and have already shown considerable scope for property tuning by appropriate substitution. We have extended the range of compounds available to include strontium manganese copper oxysulfides with thicker copper sulfide layers, and these are metamagnetic, exhibiting bulk ferromagnetic behavior when small to moderate magnetic fields are applied which invites further investigation. The thick copper sulfide layers closely resemble fragments of the fast ion-conducting phase α-Cu_2S; the intergrowth structure of these compounds constrains the basal lattice parameter and results in larger than ideal tetrahedral sites for the copper ions, resulting in copper ion disorder and possible high copper ion mobility. These compounds invite further detailed investigations. The detailed correlation of the low-temperature structures and the magnetic and electronic properties of these phases will be essential for determining the origin of the low-temperature structural distortions. More widely, there are numerous possibilities for control of the electron count and properties using chemical substitution at nearly every crystallographic site in these and related structures.

Acknowledgment. We thank the UK EPSRC for funding under Grant GR/N18758 and for providing access to the ISIS facility, the SRS, and the ILL. TEM measurements were performed within the framework of the IAP 5-1 of the Belgian government. We thank: Dr. N. Charnley (Department of Earth Sciences, University of Oxford) for assistance with EDX analysis; Dr. R. I. Smith (ISIS facility) and Dr. A. Hewat, Dr. E. Suard, and Mr. L. Gendrin (ILL, Grenoble) for assistance with PND investigations; Dr. A. T. Boothroyd and Dr. D. Prabhakaran (Department of Physics, University of Oxford) for high field magnetic susceptibility measurements; Dr. K. Takase, Department of Physics, Nihon University, Japan for measuring the Seebeck coefficient of one of the samples; Dr. M. A. Hayward (Inorganic Chemistry Laboratory, Oxford) for providing the sample of $CaMnO_3$ for XANES studies.

Supporting Information Available: Crystallographic data in CIF format for $Sr_2MnO_2Cu_{1.5}S_2$ (240 K), $Sr_2MnO_2Cu_{3.5}S_3$ (293 K), $Sr_2MnO_2Cu_{5.5}S_4$ (150 and 293 K), and $Sr_4Mn_2O_4Cu_5S_5$ (293 K); tables of refined atomic coordinates from SXRD and PND refinements (Tables S1−S5); results of fits to magnetic susceptibility data (Table S6). This material is available free of charge via the Internet at http://pubs.acs.org.

JA060892O

(51) Rutt, O. J.; Williams, G. R.; Clarke, S. J. *Chem. Commun.* **2006**. DOI: 10.1039/b605105g.